

Article

A Molecular Electron Density Theory Study of the [3+2] Cycloaddition Reaction of an Azomethine Ylide with an Electrophilic Ethylene Linked to Triazole and Ferrocene Units

 Luis R. Domingo ^{1,*}, Mar Ríos-Gutiérrez ¹  and Assem Barakat ² 
¹ Department of Organic Chemistry, University of Valencia, Dr. Moliner 50, 46100 Burjassot, Valencia, Spain

² Department of Chemistry, College of Science, King Saud University, P.O. Box 2455, Riyadh 11451, Saudi Arabia

* Correspondence: luisrdomingo@gmail.com

Abstract: The [3+2] cycloaddition (32CA) reaction of an azomethine ylide (AY) with an electrophilic ethylene linked to triazole and ferrocene units has been studied within the Molecular Electron Density Theory (MEDT) at the ω B97X-D/6-311G(d,p) level. The topology of the electron localization function (ELF) of this AY allows classifying it as a *pseudo(mono)radical* species characterized by the presence of two monosynaptic basins, integrating a total of 0.76 e, at the C1 carbon. While the ferrocene ethylene has a strong electrophilic character, the AY is a supernucleophile, suggesting that the corresponding 32CA reaction has a high polar character and a low activation energy. The most favorable *ortho/endo* reaction path presents an activation enthalpy of 8.7 kcal·mol⁻¹, with the 32CA reaction being exergonic by -42.1 kcal·mol⁻¹. This reaction presents a total *endo* stereoselectivity and a total *ortho* regioselectivity. Analysis of the global electron density transfer (GEDT) at the most favorable **TS-on** (0.23 e) accounts for the high polar character of this 32CA reaction, classified as forward electron density flux (FEDF). The formation of two intermolecular hydrogen bonds between the two interacting frameworks at the most favorable **TS-on** accounts for the unexpected *ortho* regioselectivity experimentally observed.

Keywords: Molecular Electron Density Theory (MEDT); [3+2] cycloaddition (32CA); azomethine ylide (AY); spirooxindoles; ferrocene; triazole



Citation: Domingo, L.R.; Ríos-Gutiérrez, M.; Barakat, A. A Molecular Electron Density Theory Study of the [3+2] Cycloaddition Reaction of an Azomethine Ylide with an Electrophilic Ethylene Linked to Triazole and Ferrocene Units. *Molecules* **2022**, *27*, 6532. <https://doi.org/10.3390/molecules27196532>

Academic Editor: Alistair J. Lees

Received: 12 September 2022

Accepted: 28 September 2022

Published: 3 October 2022

Publisher's Note: MDPI stays neutral with regard to jurisdictional claims in published maps and institutional affiliations.



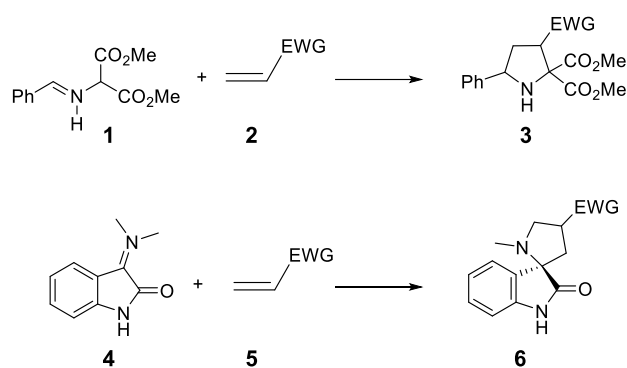
Copyright: © 2022 by the authors. Licensee MDPI, Basel, Switzerland. This article is an open access article distributed under the terms and conditions of the Creative Commons Attribution (CC BY) license (<https://creativecommons.org/licenses/by/4.0/>).

1. Introduction

The construction of enantiomerically pure compounds has experienced a significant progress during recent decades by asymmetric reactions using organocatalysis, chiral substrates/auxiliaries, and reagents able to control the stereochemistry of desired enantioselective molecules. To synthesize pharmacologically active chiral molecules for specific receptors or proteins, the establishment of structure–function relationships and mechanistic studies are indispensable. The [3+2] cycloaddition (32CA) reactions, which have proved to be highly selective, efficient, environment-friendly and atom-economical, are among the most efficient asymmetric reactions to construct pharmacologically active chiral molecules in a regio- and/or stereoselective fashion [1–4].

Organic chemists have been extensively made great efforts to understand the electronic structure of three-atom-components (TACs) generated in situ as intermediates in 32CA reactions. Based on the recently proposed Molecular Electron Density Theory (MEDT) [5], four different types of TACs, namely zwitterionic (zw), carbenoid (cb), *pseudo(mono)radical* (pmr), and *pseudodiradical* (pdr) TACs, and their reactivity towards ethylene have been characterized [6]. Notably, *pseudo(mono)radical* and *pseudodiradical* TACs are very reactive due to their instability. These electronic structures and the corresponding reactivities can be modified by substitution.

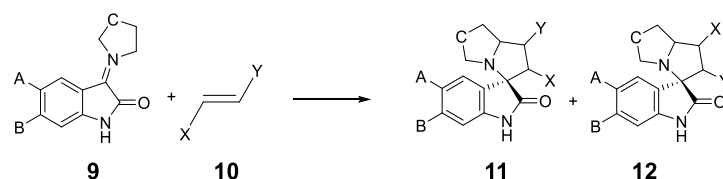
Pyrrolidines are five-membered heterocyclic compounds used as pharmacologically relevant scaffolds in drug design [7–9], which can be easily constructed by 32CA reaction of AYs with olefins (see Scheme 1). On the other hand, the introduction of a spiro-ring in heterocyclic compounds is a widely used strategy in drug design to provide additional conformational restriction. Thus, the 32CA reaction of exocyclic AY **4** generated from isatin, i.e., a dicarbonyl compound, yields spirooxindoles **6**, which possesses significant pharmacological properties [10–14].



Scheme 1. Synthesis of pyrrolidines **3** and spirooxindoles **6** by 32CA reactions of AYs.

MEDT studies of the 32CA reactions of the simplest AY **7**, $\text{CH}_2\text{-NH-CH}_2$ [15], and carbonyl ylide **8**, $\text{CH}_2\text{-O-CH}_2$ [16], have shown that the presence of a *pseudoradical* center at each one of the two methylene carbons of these TACs causes the corresponding *pdr-type* 32CA reactions with non-activated ethylenes to have an unappreciable activation energy, lower than $1.0 \text{ kcal}\cdot\text{mol}^{-1}$. However, the presence of an electron-releasing phenyl group and electron-withdrawing (EW) carboxyl $\text{-CO}_2\text{R}$ or nitrile -CN groups at the two methylenes of the simplest AY **7**, just as AY **1**, stabilizes its *pseudodiradical* electronic structure, modifying the experimental reactivity of these substituted AYs to that of *pseudo(mono)diradical* [17], carbenoid [18], or even zwitterionic TACs [19].

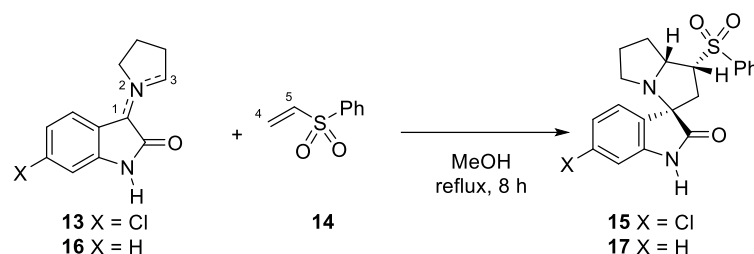
Recently, Barakat and co-workers experimentally studied the synthesis of spirooxindoles **11** and **12** via 32CA reactions of AYs **9**, generated from substituted isatins and secondary amines, with disubstituted olefins, in excellent regio- and stereoselectivity (see Scheme 2) [20–22]. The plausible reaction mechanism was suggested to take place via an *endo* stereoisomeric path in which the substitution of the olefin derivatives **10** plays a crucial role in the regioselective formation of the products **11** or **12**.



Scheme 2. 32CA reactions of AYs **9** derived from indol-2,3-diones.

Thus, the 32CA reaction of AY **13** with phenyl vinyl sulphone **14** yields the spirooxindole **15** with total *meta* regio- and *endo* stereoselectivity (see Scheme 3) [23]. A MEDT study of the 32CA reaction of model AY **16** with phenyl vinyl sulphone **14** [24] showed that this 32CA reaction takes place via a *two-stage one-step* [25] mechanism involving a highly asynchronous transition-state structure (TS), with a high *endo* stereoselectivity and high *meta* regioselectivity. The reaction presents a very low activation enthalpy, $5.7 \text{ kcal}\cdot\text{mol}^{-1}$, as a consequence of the strong polar character of the reaction; the global electron density transfer (GEDT) [26] at the most favorable *meta/endo* TS was 0.31 e. This behavior is a consequence of the supernucleophilic character of AY **16** and the strong electrophilic character of vinyl sulphone **14**. The *meta* regioselectivity was explained by the more favorable

two-center interaction between the most nucleophilic center of AY 16, the C1 carbon, and the more electrophilic center of phenyl vinyl sulphone 14, the C4 carbon, anticipated by the analysis of the Parr functions [27].

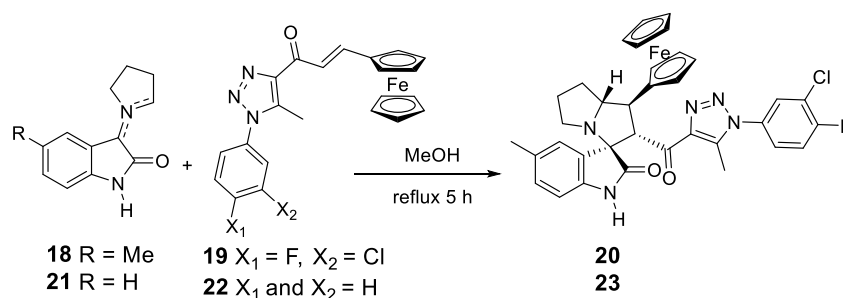


Scheme 3. 32CA reaction of AY 13 with phenyl vinyl sulphone 14 yielding spirooxindole 15 regio- and stereoselectively.

The ferrocene scaffold is an interesting organometallic architecture with a diversity of applications in medicine, photochemistry, as well as a building block for many organic synthetic transformations [28–31]. Many synthesized or naturally occurring organic compounds incorporating the ferrocene unit possess pharmacological activity which is sold in the market or in more advanced preclinical stages. Introducing the ferrocene synthon into the spirooxindoles scaffold is challenging for experimental chemists.

Triazoles, in particular the 1,2,3-triazole motif, have attracted great deal of attention due to their biological activities as anti-malarial agents, carbonic anhydrase inhibitors, agents for the tuberculosis treatment, etc., [32–44]. Introducing another interesting pharmacophore such as the 1,2,3-triazole framework into the spirooxindoles in combination with the ferrocene organometallic unit may lead to particular properties that could be useful for different applications in varied fields such as supramolecular chemistry, biochemistry, biosensing probes, or conducting polymer chemistry.

Very recently, Barakat et al. have experimentally reported the 32CA reaction of AY 18 with ethylene derivative 19, in the synthesis of spirooxindoles 20, with high *ortho* regio- and *endo* stereoselectivity (see Scheme 4) [45]. Interestingly, this 32CA shows an opposite regioselectivity to that shown in the reaction with vinyl sulphone 14 (see Scheme 3).



Scheme 4. 32CA reaction of AY 18 with ferrocene ethylene 19, yielding spirooxindole 20 *ortho* regio- and *endo* stereoselectively.

Herein, the 32CA reaction of AY 21 with ferrocene ethylene 22 yielding spirooxindole 23, as a computational model of the 32CA reaction studied by Barakat et al., is theoretically studied within the MEDT in order to understand the behavior of the 32CA reactions involving ferrocene ethylene derivatives (see Scheme 4) and the origin of the unexpected *ortho* regioselectivity.

2. Results and Discussion

The present MEDT study has been divided in four sections: (i) first, an ELF topological analysis at the ground state of AY 21 and ferrocene ethylene derivative 22 is performed; (ii) in the second part, the conceptual DFT (CDFT) reactivity indices at the ground state of

the reagents are analyzed; (iii) in the third part, the competitive reaction paths associated with the 32CA reaction of AY **21** with ferrocene ethylene **22** are studied; and (iv) the origin of the *ortho* regioselectivity is finally analyzed.

2.1. ELF Topological Analysis at the Ground State of AY **21** and Ferrocene Ethylene Derivative **22**

The topological analysis of the electron localization function (ELF) [46] at the ground state allows a quantitative and qualitative description of the electronic structure of organic molecules [47]. Given the structure–reactivity relationship found in TACs [6], an ELF topological analysis of AY **21** was first performed in order to characterize its electronic structure and gain some insight about its reactivity. The most significant ELF basin attractor positions and valence basin populations of AY **21** and ferrocene ethylene **22** are given in Figure 1.

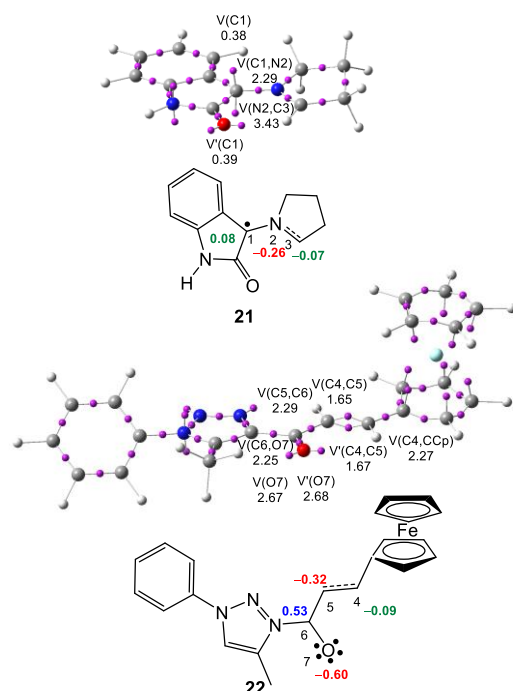


Figure 1. ω B97X-D/6-311G(d,p) ELF basin attractor positions together with the most relevant valence basin populations and ELF-based Lewis-like structures together with natural atomic charges of AY **21** and ferrocene ethylene **22**. Valence basin populations and natural atomic charges are given in average number of electrons, e. Negative charges are colored in red, positive charges in blue, and negligible charges in green.

The ELF of AY **21** shows the presence of two monosynaptic basins, V(C1) and V'(C1), integrating a total of 0.77 e, one V(C1,N2) disynaptic basin integrating 2.29 e and one V(N2,C3) disynaptic basin integrating 3.43 e, characterizing the C1–N2–C3 AY core. While the V(C1,N2) disynaptic basin is associated with a C1–N2 single bond, the V(N2,C3) disynaptic basin is associated with a somewhat underpopulated N2–C3 double bond. The presence of the two monosynaptic basins at the C1 carbon integrating less than 1.0 e, which are associated with a *pseudoradical* C1 center [15], allows the classification of AY **21** as a *pseudo(mono)radical* TAC participating in *pmr*-type 32CA reactions [6].

On the other hand, the ELF of ferrocene ethylene derivative **22** shows the presence of two disynaptic basins, V(C4,C5) and V'(C4,C5) integrating a total of 3.32 e, a V(C5,C6) disynaptic basin integrating 2.29 e, one V(C6,O7) disynaptic basin integrating 2.25 e, and two monosynaptic basins, V(O7) and V'(O7) integrating a total of 5.35 e. While the two V(C4,C5) and V'(C4,C5) disynaptic basins are associated with an underpopulated C4–C5 double bond, the V(C6,O7) disynaptic basin is associated with a carbonyl C6–O7 single

bond, resulting from a strong polarization of the C6–O7 bonding region towards the electronegative O7 oxygen, which shows a non-bonding region with a high electron density.

Natural Population Analysis (NPA) [48,49] of the charge distribution shows that the two reactive carbons of AY 21 are negligibly charged by less than ± 0.08 e while the N2 nitrogen is negatively charged by -0.26 e. Interestingly, the natural charges of ethylene derivative 22 indicate that the C4 and C5 carbons are negatively charged by -0.32 and -0.09 e, respectively while the carbonyl C6 carbon is strongly positively charged by 0.53 e as a consequence of the strong polarization of the carbonyl C6–O7 bonding region towards the electronegative O7 oxygen, which has a negative charge of -0.60 e.

2.2. CDFT Analysis at the Ground State of the Reagents

The reactivity indices defined within CDFT [50,51] have shown to be powerful tools to understand the reactivity in polar reactions [52]. The global reactivity indices, namely, the electronic chemical potential μ , chemical hardness η , electrophilicity ω , and nucleophilicity N indices, of AY 21 and ferrocene ethylene 22 are gathered in Table 1.

Table 1. B3LYP/6-31G(d) electronic chemical potential μ , chemical hardness η , electrophilicity ω , and nucleophilicity N indices, in eV, of AY 21 and ferrocene ethylene 22.

	μ	η	ω	N
ferrocene ethylene 22	-3.53	3.61	1.72	3.78
AY 21	-2.79	3.33	1.17	4.67

The electronic chemical potential [53] of AY 21 with $\mu = -2.79$ eV is higher than that of ferrocene ethylene 22 with $\mu = -3.53$ eV, indicating that along a polar 32CA reaction the GEDT [26] will take place from AY 21 to ferrocene ethylene 22, the corresponding polar 32CA reaction being classified as of forward electron density flux (FEDF) [54].

AY 21 presents an electrophilicity ω index [55] of 1.17 eV, being classified as a moderate electrophile within the electrophilicity scale [51], and a nucleophilicity N index [56] of 4.67 eV, being classified as a strong nucleophile within the nucleophilicity scale [51]. The strong nucleophilic character of AY 21, higher than 4.0 eV, allows its classification as a supernucleophile [57]. On the other hand, ferrocene ethylene 22 presents an electrophilicity ω index of 1.72 eV, being classified as a strong electrophile, and a nucleophilicity N index of 3.78 eV, being also classified as a strong nucleophile. The supernucleophilic character of AY 21, together with the strong electrophilic character of ferrocene ethylene 22, indicates that the corresponding 32CA reaction will have a high polar character, being classified as FEDF [54].

In a polar 32CA reaction involving non-symmetric species, the most favorable reaction path is that involving the two-center interaction between the most electrophilic and the most nucleophilic centers of the two reagents [58]. Many studies have shown that the electrophilic P_k^+ and nucleophilic P_k^- Parr functions [27], resulting from the excess of spin electron density gathered via the GEDT, are among the most accurate tools for the analysis of the local reactivity in polar and ionic processes [52]. Hence, according to the characteristics of the reagents, the nucleophilic P_k^- Parr functions of AY 21 and the electrophilic P_k^+ Parr functions of ferrocene ethylene 22 were analyzed (see Figure 2).

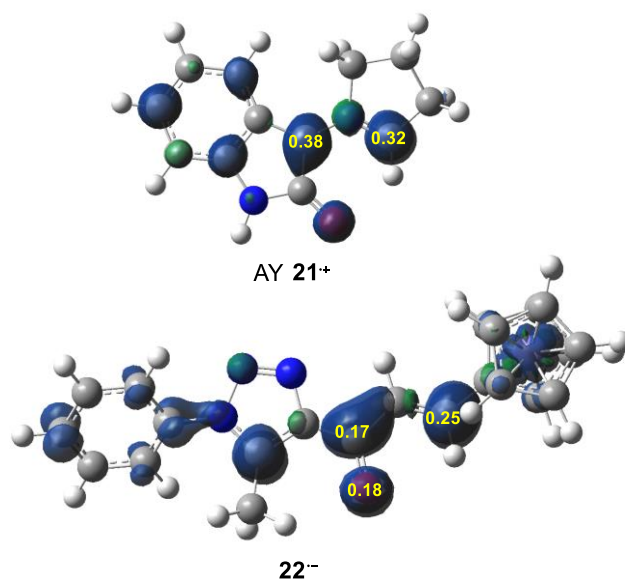


Figure 2. B3LYP/6-31G(d) nucleophilic P_k^- Parr functions of AY 21 and electrophilic P_k^+ Parr functions of ferrocene ethylene 22.

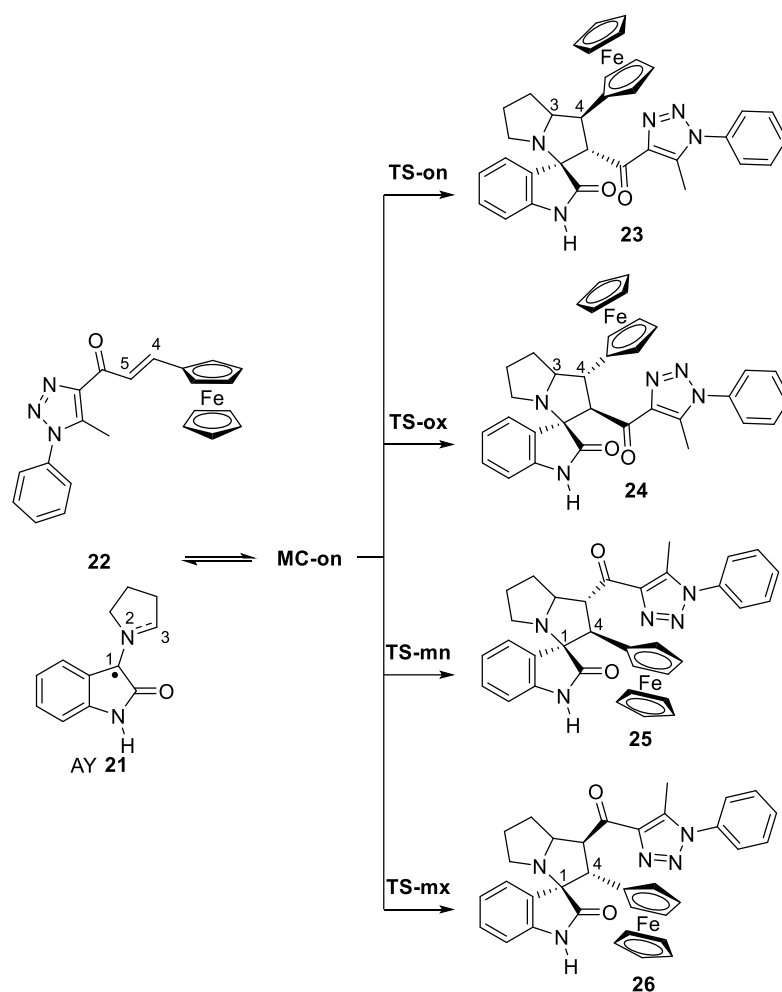
The two C1 and C3 carbons of AY 21 are nucleophilically activated by $P_k^- = 0.38$ and 0.32, respectively, with the C1 carbon being the most nucleophilic center of the TAC. Note that the N2 nitrogen is nucleophilically deactivated ($P_k^- = -0.12$). On the other hand, the β -conjugated C4 position of ferrocene ethylene 22 is the most electrophilically activated of this species ($P_k^+ = 0.25$).

Based on the analysis of the Parr functions, the *meta* regioisomer is expected to be the preferred one as a consequence of the slightly higher nucleophilic activation of the C1 carbon of AY 21 than that of the C3 one.

2.3. Analysis of the Competitive Reaction Paths Associated with the 32CA Reaction of AY 21 with Ferrocene Ethylene 22

In order to determine the mechanism of this 32CA reaction, the competitive reaction paths associated with the 32CA reaction of AY 21 with ferrocene ethylene 22 were analyzed. Due to the non-symmetry of both reagents, two pairs of *endo* and *exo* stereoisomeric reaction paths and two pairs of *ortho* and *meta* regioisomeric ones are possible (see Scheme 5). The analysis of the stationary points found along with these reaction paths indicates that this 32CA reaction takes place through a one-step mechanism. The ω B97X-D/6-311G(d,p) relative electronic energies, in gas phase and in methanol, are given in Table 2. Total electronic energies are given in Table S1 in Supplementary Materials.

An exhaustive analysis of the potential energy surface associated with this 32CA reaction allowed finding a series of molecular complexes (MCs), which are in equilibrium, in an early stage of the reaction. The most favorable **MC-on**, which opens the *ortho/endo* reaction path, is found to be 25.6 kcal·mol⁻¹ more stable than the separated reagents (see Scheme 5).



Scheme 5. Competitive reaction paths associated with the 32CA reaction of AY **21** and ferrocene ethylene **22**.

Table 2. ω B97X-D/6-311G(d,p) relative energies, in kcal·mol⁻¹, in gas phase and in methanol, of the stationary points involved in the 32CA reaction of AY **21** with ferrocene ethylene **22**.

	Gas Phase	Methanol
MC-on	-25.6	-20.6
TS-on	-17.1	-11.2
TS-ox	-8.8	-6.3
TS-mn	-11.8	-7.2
TS-mx	-6.7	-2.9
23	-49.9	-45.2
24	-44.2	-39.8
25	-51.9	-46.0
26	-55.1	-49.7

Some appealing conclusions can be obtained from the analysis of the relative energies of the stationary points involved in this 32CA reaction: (i) the most favorable **TS-on** is found to be 17.1 kcal·mol⁻¹ below the separate reagents; (ii) however, when the formation of **MC-on** is considered, the activation energy of this 32CA reaction becomes positive at 8.5 kcal·mol⁻¹; (iii) this 32CA reaction is strongly exothermic by -49.9 kcal·mol⁻¹. Consequently, the formation of the experimental spirooxindole **23** takes place by kinetic control. Note that the reaction is strongly exergonic by -22.4 kcal·mol⁻¹ (see later); (iv) this 32CA reaction is completely *ortho* regioselective, as **TS-mn** is found to be 5.3 kcal·mol⁻¹

above **TS-on**; and (v) this 32CA reaction is completely *endo* stereoselective, as **TS-ox** is found to be $8.3 \text{ kcal}\cdot\text{mol}^{-1}$ above **TS-on**.

Inclusion of solvent effects of methanol stabilizes all species by between 15.3 and $19.7 \text{ kcal}\cdot\text{mol}^{-1}$; the reagents are the most stabilized [59]. As a consequence, the relative energies of the TSs increase by between 2.5 and $5.9 \text{ kcal}\cdot\text{mol}^{-1}$. In methanol, the activation energy increases by $0.9 \text{ kcal}\cdot\text{mol}^{-1}$, and the 32CA reaction remains completely regio- and stereoselective, as **TS-mn** and **TS-ox** are found to be 4.0 and $5.0 \text{ kcal}\cdot\text{mol}^{-1}$, respectively, above **TS-on**. The 32CA reaction remains strongly exothermic by $-45.2 \text{ kcal}\cdot\text{mol}^{-1}$.

The ω B97X-D/6-311G(d,p) thermodynamic data of the 32CA reaction of AY **21** with ferrocene ethylene **22** were further analyzed. The relative enthalpies, entropies, and Gibbs free energies are given in Table 3, while the thermodynamic data are given in Table S2 in Supplementary Materials.

Table 3. ω B97X-D/6-311G(d,p) relative enthalpies (ΔH , $\text{kcal}\cdot\text{mol}^{-1}$), entropies (ΔS , $\text{cal}\cdot\text{mol}^{-1}\cdot\text{K}^{-1}$), and Gibbs free energies (ΔG , $\text{kcal}\cdot\text{mol}^{-1}$), computed at $65 \text{ }^\circ\text{C}$ in methanol, of the stationary points involved in the 32CA reaction of AY **21** with ferrocene ethylene **22**.

	ΔH	ΔS	ΔG
MC-on	-18.8	-48.4	-2.5
TS-on	-10.1	-59.8	10.1
TS-ox	-5.2	-58.1	14.5
TS-mn	-6.4	-50.3	10.6
TS-mx	-2.1	-47.6	14.0
23	-42.1	-58.2	-22.4
24	-36.6	-59.4	-16.5
25	-42.7	-54.7	-24.2
26	-46.7	-60.2	-26.3

A representation of the enthalpy and Gibbs free energy profiles associated with the four competitive reaction paths is given in Figure 3. The inclusion of the thermal corrections to the electronic energies in methanol increases the relative enthalpies only by between 0.8 and $3.4 \text{ kcal}\cdot\text{mol}^{-1}$. Indeed, they have a markedly low incidence in the relative enthalpies of the TSs, which only increase by between 0.8 and $1.1 \text{ kcal}\cdot\text{mol}^{-1}$ with respect to the electronic energies in methanol. Considering the activation enthalpies, **TS-ox** and **TS-mx** are found to be more than $3.7 \text{ kcal}\cdot\text{mol}^{-1}$ higher in enthalpy than **TS-on**. The inclusion of entropies to enthalpies increases the relative Gibbs free energies by between 16.1 and $20.3 \text{ kcal}\cdot\text{mol}^{-1}$ as a consequence of the unfavorable activation entropies associated with these bimolecular processes, which are found in the range -47.6 and $-60.2 \text{ cal}\cdot\text{mol}^{-1}\cdot\text{K}^{-1}$, and the temperature of the reaction of $65 \text{ }^\circ\text{C}$. The formation of **MC-on** is exergonic by $-2.5 \text{ kcal}\cdot\text{mol}^{-1}$. The activation Gibbs free energy associated with this 32CA reaction via **TS-on** rises to $12.6 \text{ kcal}\cdot\text{mol}^{-1}$, while the formation of spirooxindole **23** is strongly exergonic by $-22.4 \text{ kcal}\cdot\text{mol}^{-1}$.

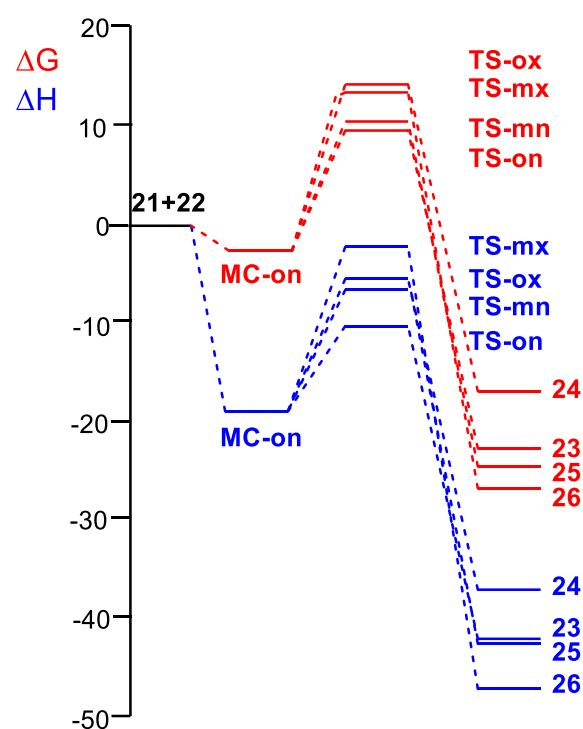


Figure 3. ω B97X-D/6-311G(d,p) enthalpy ΔH in kcal mol⁻¹ (blue) and Gibbs free energy ΔG in kcal mol⁻¹ (red) profiles, at 65 °C in methanol, for the 32CA reaction of AY **21** with ferrocene ethylene **22**.

It is interesting to highlight that while the activation enthalpies suggest that this 32CA reaction is completely *ortho* regioselective, in full agreement with the experimental outcomes [45], the activation Gibbs free energies markedly decrease the *ortho* regioselectivity as **TS-mn** is only 0.5 kcal·mol⁻¹ above **TS-on**. This behavior is a consequence of the more unfavorable activation entropy associated with the *ortho* TSs (see later).

The geometries of **MC-on** and the four TSs are given in Figures 4 and 5, respectively. At **MC-on**, the two interacting frameworks, which are separated by a distance of ca. 3.11 Å, present a parallel rearrangement (see Figure 4). At the more favorable *ortho* TSs, the distances between the two pairs of C3–C4 and C1–C5 interacting carbons are 2.112 and 2.704 Å, respectively, at **TS-on** and 2.126 and 2.562 Å, respectively, at **TS-ox**, while at the *meta* TSs, the distances between the two pairs of C1–C4 and C3–C5 interacting carbons are: 2.081 and 2.633 Å, respectively, at **TS-mn** and 2.320 and 2.268 Å, respectively, at **TS-mx** (see Figure 5). These distances indicate that while the most favorable **TS-on** shows a high geometrical asynchronicity with $\Delta l = 0.59$ Å, the most unfavorable **TS-mx** shows a very low geometrical asynchronicity with $\Delta l = 0.05$ Å. The most favorable highly asynchronous **TS-on** is associated with a two-center interaction between the C3 carbon of AY **21**, the second most nucleophilic center of this TAC, and the β -conjugated C4 carbon of ferrocene ethylene **22**, the most electrophilic center of this ethylene derivative.

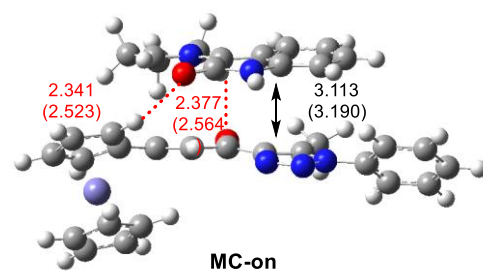


Figure 4. ω B97X-D/6-311G(d,p) optimized geometry of **MC-on**. Distances are given in angstroms, Å. Distances in methanol are given in parentheses. HB distances are given in red.

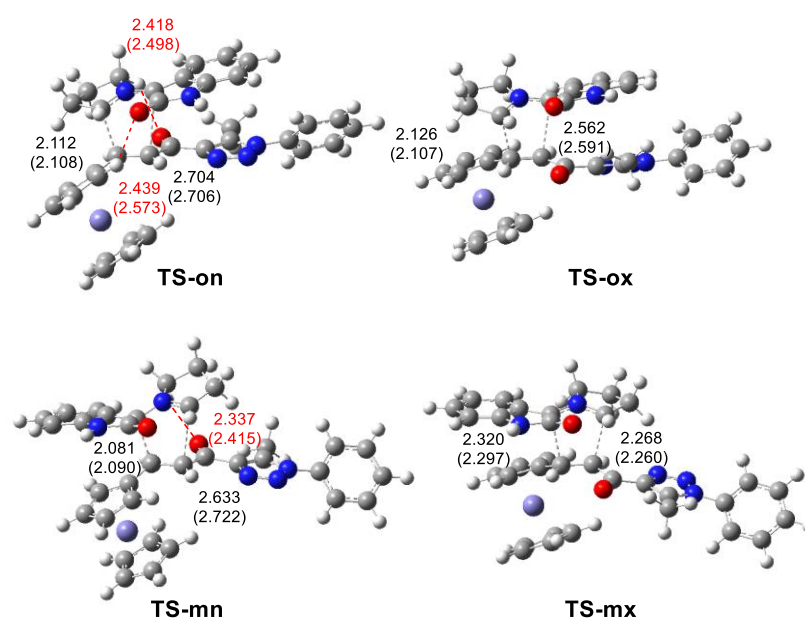


Figure 5. ω B97X-D/6-311G(d,p) optimized geometries of the TSs associated with the 32CA reaction of AY **21** with ferrocene ethylene **22**. Distances are given in angstroms, Å. Distances in methanol are given in parentheses. HB distances are given in red.

A detailed analysis of the geometry of the most favorable **TS-on** shows that one of the hydrogens of the ferrocene framework of ethylene **22** is located at 2.439 Å of the carbonyl oxygen atom of AY **21**, and one hydrogen of the dihydropyrrole ring of AY **21** is located at 2.418 Å of the carbonyl oxygen atom of ferrocene ethylene **22** (see Figure 5). These distances suggest the presence of two hydrogen bonds (HBs) between the hydrogen and oxygen centers. Interestingly, these HBs which are already present at the most stable **MC-on**, with H–O distances of 2.341 and 2.377 Å, respectively (see Figure 4), may account for the *ortho* and *endo* selectivity found in this 32CA reaction. The formation of these HBs, with the first one exhibited by a slight twist of the cyclopentadienyl ring with respect to the C4–C5 double bond, could be responsible for the lower entropy associated with **TS-on**, i.e., 230.2 cal·mol^{−1}·K^{−1}, than that of **TS-mn**, i.e., 239.7 cal·mol^{−1}·K^{−1} (see Table S2 in Supplementary Material) and, consequently, for the loss of *ortho* regioselectivity when relative Gibbs free energies are considered (see Table 3).

On the other hand, the analysis of the geometry of the regioisomeric **TS-mn** suggests the presence of only one HB between the carbonyl O7 oxygen of ferrocene ethylene **22** and one of the dihydropyrrole hydrogen of AY **21**, with a H–O distance of 2.337 Å (see Figure 5). Thus, the presence of an additional HB at the most favorable **TS-on** accounts for the change of regioselectivity in this 32CA reaction.

Finally, the analysis of the GEDT [26] at **TS-on** permits the assessment of the polar character of this 32CA reaction. GEDT values lower than 0.05 e correspond to non-polar processes, while GEDT values higher than 0.20 e correspond to high polar processes. The GEDT value at the two stereoisomeric *ortho* TSs is 0.23 e. This high value is a consequence of the supernucleophilic character of AY **21** and the strong electrophilic character of ferrocene ethylene **22**. The flux of the electron density, which goes from AY **21** to ferrocene ethylene **22**, allows classifying this 32CA reaction as FEDF, in clear agreement with the analysis of the CDFT indices. The high polar character of this 32CA reaction accounts for the fact that, considering the relative enthalpies, **TS-on** is located below the separated reagents (see Table 3) [60].

Figure 6 shows the ELF [46] basin attractor positions of **MC-on** and **TS-on**. The ELF of **MC-on** presents similar features to those of the separate reagents, i.e., AY **21** and ferrocene ethylene **22** (see Figure 1). The AY framework of **MC-on** shows the presence of one V(C1) monosynaptic basin, integrating 0.33 e, already present at *pseudo(mono)radical* AY **1**, while

the C4–C5 double bond of the ferrocene ethylene moiety is characterized by the presence of two disynaptic basins, $V(C4,C5)$ and $V'(C4,C5)$, integrating a total of 3.27 e (see Figures 1 and 6).

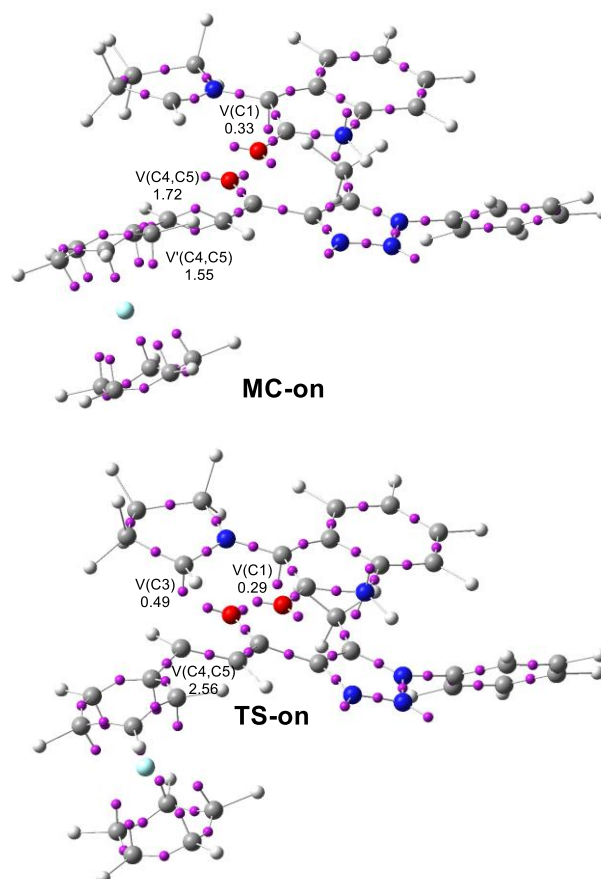


Figure 6. ω B97X-D/6-311G(d,p) ELF basin attractor positions together with the populations of the most relevant valence basins of **MC-on** and **TS-on**. Valence basin populations are given in average number of electrons (e).

The most relevant feature of **TS-on** is the creation of a new $V(C3)$ monosynaptic basin integrating 0.49 e, while the $V(C1)$ monosynaptic basins present at **MC-on** is slightly depopulated to 0.29 e. This new monosynaptic basin, which is created at the second most nucleophilic center of AY **21** (see Parr functions in Figure 2), is demanded for the subsequent creation of the first new C3–C4 single bond [26]. On the other hand, the two disynaptic basins associated with the C4–C5 partial double bond present at ferrocene ethylene **22** and **MC-on** merge into one single $V(C4-C5)$ disynaptic basin at **TS-on** after losing 0.71 e from ethylene **22**. This ELF analysis of **TS-on**, which accounts for the non-concerted nature of this one-step 32CA reaction, supports the previous analysis based on the geometrical parameters.

2.4. Origin of the *Ortho/Endo* Regioselectivity

As has been aforementioned, the geometries of the more favorable **MC-on** and **TS-on** suggest the presence of two HBs between the carbonyl oxygen atoms and the ring hydrogen atoms, which might be responsible for the unexpected *ortho* regioselectivity (see Figures 4 and 5). Thus, in order to confirm their presence, a topological analysis of the electron density associated with the intermolecular non-covalent interactions (NCI) taking place at both stationary points was performed by means of the Independent Gradient Model [61,62] (IGM). The corresponding isosurfaces are represented in Figure 7.

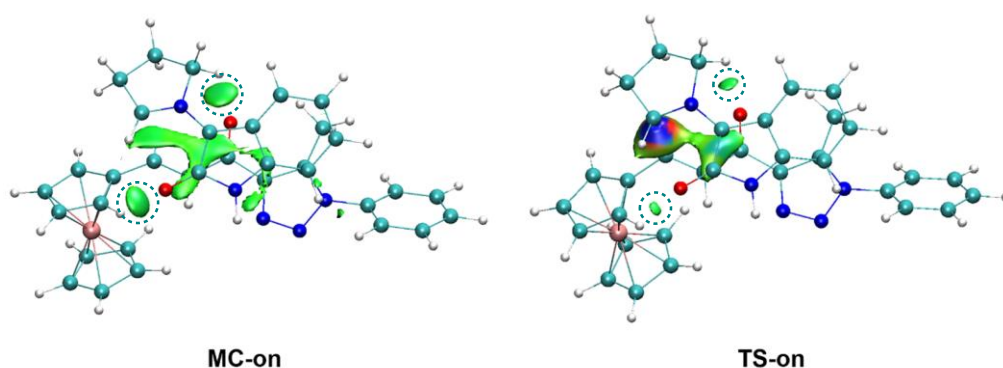


Figure 7. IGM- δg_{inter} 0.010 a.u. (**MC-on**) and 0.018 a.u. (**TS-on**) isosurfaces, represented with a blue-green-red color-code in the range of $-0.08 < (\text{sign}) \lambda_2 \rho < 0.08$ a.u. The attractive IGM- δg_{inter} surfaces associated with the two HBs are highlighted by a line-dashed green circle.

IGM- δg_{inter} at **MC-on** shows a green surface between the main interacting regions of both AY and ethylene frameworks and two additional green surfaces involving the two carbonyl oxygen atoms and one of the cyclopentadienyl or dihydropyrrole hydrogen atoms. While the more extended surface is related to the non-covalent interactions in the bond formation region, which turns to a blue-to-red color at **TS-on** as a consequence of the higher proximity between the two frameworks and the more advanced C3–C4 bond formation, the two surfaces in the O–H regions are related to weak HBs with δg_{inter} signatures and intrinsic bond strength index (IBSI) [63] values of ca. 0.03 a.u. These surfaces become smaller, and the respective HBs weaker, at **TS-on** due to a slight elongation of the corresponding O–H distances by 0.065 and 0.013 Å. Although their contributions to the intermolecular interactions [64] are lower than 4%, with the O(Et)–H(AY) interaction contributing 0.6% more than the O(AY)–H(Et) interaction, their presence seems to outweigh the more favorable electrophilic/nucleophilic electronic interactions involving the most nucleophilic C1 *pseudoradical* center along the *meta/endo* path [24], thus leading to the *ortho/endo* selectivity.

Finally, the IGM- δg_{inter} at the regioisomeric **TS-mn** shows the presence of only one HB between the carbonyl O7 oxygen of ferrocene ethylene **22** and one of the dihydropyrrole hydrogens of AY **21** (see Figure S1 in Supplementary Material). Consequently, the additional HB present at the most favorable **TS-on** can explain the fact that this TS is 5.4 kcal·mol^{−1} more stable than **TS-mn**, and, consequently, the origin of the unexpected *ortho* regioselectivity of this 32CA reaction [45].

3. Materials and Methods

The ω B97X-D [65] functional, together with the standard 6-311G(d,p) basis set [66], which includes d-type polarization for second-row elements and p-type polarization functions for hydrogen atoms, were used in this MEDT study. The TSs were characterized by the presence of only one imaginary frequency. The Bery method was used in optimizations [67,68]. The IRC [69] calculations were performed to establish the unique connection between the TSs and the corresponding minima [70,71] phase structures at the same computational level using the polarizable continuum model (PCM) [72,73] in the framework of the self-consistent reaction field (SCRf) [74–76]. Values of ω B97X-D/6-311G(d,p) enthalpies, entropies, and Gibbs free energies in methanol were calculated with standard statistical thermodynamics at 337.8 K and 1 atm [66], by PCM frequency calculations at the solvent optimized structures.

The GEDT [26] values were computed by using the equation $\text{GEDT}(f) = \sum q_f$, where q are the natural charges [48,49] of the atoms belonging to one of the two frameworks (f) at the TS geometries. Global and local CDFT indices [50,51] were calculated by using the equations given in reference [51], using the B3LYP/6-31G(d) method, because the original nucleophilicity and electrophilicity scales were established at that level [51].

The Gaussian 16 suite of programs was used to perform the calculations [77]. ELF [46] analyses of the ω B97X-D/6-311G(d,p) monodeterminantal wavefunctions were performed by using the TopMod [78] package with a cubical grid of step size of 0.1 Bohr. Molecular geometries and ELF basin attractors were visualized by using the GaussView program [79]. IGM analysis was carried out with the IGMPLOT software [62].

4. Conclusions

The 32CA reaction of AY 21, derived from isatin and L-proline, with ferrocene ethylene 22, yielding spirooxindole 23, has been studied within MEDT at the ω B97X-D/6-311G(d,p) computational level. Analysis of the ELF topology of AY 21 indicated that this TAC has a *pseudo(mono)radical* structure characterized by the presence of two monosynaptic basins, integrating a total of 0.77 e, at the C1 carbon. The analysis of the CDFT reactivity indices indicated that ferrocene ethylene 22 has a strong electrophilic characteristic, while AY 21 is a supernucleophile, suggesting that the corresponding 32CA reaction has a high polar character. The most favorable reaction path via the *ortho/endo* TS-on presents an activation enthalpy of 8.7 kcal·mol⁻¹, with the 32CA reaction being strongly exothermic by -42.1 kcal·mol⁻¹. Analysis of the activation enthalpies indicated that this reaction presents a complete *endo* stereoselectivity and a complete *ortho* regioselectivity, in agreement with the experimental outcomes. Analysis of the GEDT at the most favorable TS-on, 0.23 e, accounts for the high polar character of this 32CA reaction, classified as FEDF. The presence of two HBs between the two carbonyl oxygens and the two ring hydrogens at the most favorable TS-on, which are already present at MC-on, appear to be responsible for the unexpected *ortho* regio- and *endo* stereoselectivity found in this 32CA reaction involving the *pseudo(mono)radical* AY 21.

Supplementary Materials: The following supporting information can be downloaded at: <https://www.mdpi.com/article/10.3390/molecules27196532/s1>. Figure S1: IGM- $\delta_{g_{inter}}$ isosurface of TS-mn. Table S1: Total electronic energies. Table S2: Thermodynamic data. Cartesian coordinates of the stationary points involved in the 32CA reaction of AY 21 with ferrocene ethylene 22.

Author Contributions: Conceptualization, L.R.D. and M.R.-G.; methodology, L.R.D. and M.R.-G.; investigation, L.R.D., A.B. and M.R.-G.; resources, L.R.D. and M.R.-G.; writing—original draft preparation, L.R.D.; writing—review and editing, M.R.-G. and A.B.; supervision, L.R.D.; funding acquisition, L.R.D., M.R.-G. and A.B. All authors have read and agreed to the published version of the manuscript.

Funding: This work has been supported by the Ministry of Science and Innovation (MICINN) of the Spanish Government (project PID2019-110776GB-I00 (AEI/FEDER, UE)). The authors would like to extend their sincere appreciation to the Researchers Supporting Project (RSP-2021/64), King Saud University, Riyadh, Saudi Arabia.

Institutional Review Board Statement: Not applicable.

Informed Consent Statement: Not applicable.

Data Availability Statement: Not applicable.

Acknowledgments: This work has been supported by the Ministry of Science and Innovation (MICINN) of the Spanish Government, project PID2019-110776GB-I00 (AEI/FEDER, UE). The authors would like to extend their sincere appreciation to the Researchers Supporting Project (RSP-2021/64), King Saud University, Riyadh, Saudi Arabia.

Conflicts of Interest: The authors declare no conflict of interest.

Sample Availability: Cartesian coordinates of the stationary points are available in Supplementary Material.

References

1. Carruthers, W. *Some Modern Methods of Organic Synthesis*, 2nd ed.; Cambridge University Press: Cambridge, UK, 1978.
2. Padwa, A. *1,3-Dipolar Cycloaddition Chemistry*; Wiley-Interscience: New York, NY, USA, 1984; Volume 1–2.

3. Carruthers, W. *Cycloaddition Reactions in Organic Synthesis*; Pergamon: Oxford, UK, 1990.
4. Padwa, A.; Pearson, W.H. *Synthetic Applications of 1,3-Dipolar Cycloaddition Chemistry Toward Heterocycles and Natural Products*; John Wiley & Sons Inc.: New York, NY, USA, 2002; Volume 59.
5. Domingo, L.R. Molecular Electron Density Theory: A Modern View of Reactivity in Organic Chemistry. *Molecules* **2016**, *21*, 1319. [[CrossRef](#)] [[PubMed](#)]
6. Ríos-Gutiérrez, M.; Domingo, L.R. Unravelling the Mysteries of the [3 + 2] Cycloaddition Reactions. *Eur. J. Org. Chem.* **2019**, *2019*, 267–282. [[CrossRef](#)]
7. Bailly, C. Lamellarins, from A to Z: A family of anticancer marine pyrrole alkaloids. *Curr. Med. Chem. Anti-Cancer Agents* **2004**, *4*, 363–378. [[CrossRef](#)] [[PubMed](#)]
8. Bellina, F.; Rossi, R. Synthesis and biological activity of pyrrole, pyrroline and pyrrolidine derivatives with two aryl groups on adjacent positions. *Tetrahedron* **2006**, *62*, 7213–7256. [[CrossRef](#)]
9. Narayan, R.; Potowski, M.; Jia, Z.-J.; Antonchick, A.P.; Waldmann, H. Catalytic Enantioselective 1,3-Dipolar Cycloadditions of Azomethine Ylides for Biology-Oriented Synthesis. *Acc. Chem. Res.* **2014**, *47*, 1296–1310. [[CrossRef](#)] [[PubMed](#)]
10. Barakat, A.; Islam, M.S.; Ali, M.; Al-Majid, A.M.; Alshahrani, S.; Alamary, A.S.; Yousuf, S.; Choudhary, M.I. Regio- and Stereoselective Synthesis of a New Series of Spirooxindole Pyrrolidine Grafted Thiochromene Scaffolds as Potential Anticancer Agents. *Symmetry* **2021**, *13*, 1426. [[CrossRef](#)]
11. Boudriga, S.; Haddad, S.; Murugaiyah, V.; Askri, M.; Knorr, M.; Strohmam, C.; Golz, C. Three-Component Access to Functionalized Spiropyrrolidine Heterocyclic Scaffolds and Their Cholinesterase Inhibitory Activity. *Molecules* **2020**, *25*, 1963. [[CrossRef](#)]
12. Barakat, A.; Soliman, S.M.; Alshahrani, S.; Islam, M.S.; Ali, M.; Al-Majid, A.M.; Yousuf, S. Synthesis, X-ray Single Crystal, Conformational Analysis and Cholinesterase Inhibitory Activity of a New Spiropyrrolidine Scaffold Tethered Benzo[b]Thiophene Analogue. *Crystals* **2020**, *10*, 120. [[CrossRef](#)]
13. Barakat, A.; Alshahrani, S.; Al-Majid, A.M.; Ali, M.; Altowyan, M.S.; Islam, M.S.; Alamary, A.S.; Ashraf, S.; Ul-Haq, Z. Synthesis of a New Class of Spirooxindole–Benzo[b]Thiophene-Based Molecules as Acetylcholinesterase Inhibitors. *Molecules* **2020**, *25*, 4671. [[CrossRef](#)]
14. Barakat, A.; Al-Majid, A.M.; Lotfy, G.; Ali, M.; Mostafa, A.; Elshaier, Y.A.; Al-Habib, S. Drug Repurposing of Lactoferrin Combination in a Nanodrug Delivery System to Combat Severe Acute Respiratory Syndrome Coronavirus-2 Infection. *Med. J.* **2021**, *3*, 104–112. [[CrossRef](#)]
15. Domingo, L.R.; Chamorro, E.; Pérez, P. Understanding the High Reactivity of the Azomethine Ylides in [3 + 2] Cycloaddition Reactions. *Lett. Org. Chem.* **2010**, *7*, 432–439. [[CrossRef](#)]
16. Domingo, L.R.; Sáez, J.A. Understanding the Electronic Reorganization along the Nonpolar [3 + 2] Cycloaddition Reactions of Carbonyl Ylides. *J. Org. Chem.* **2011**, *76*, 373–379. [[CrossRef](#)] [[PubMed](#)]
17. Domingo, L.R.; Ríos-Gutiérrez, M.; Pérez, P. A Molecular Electron Density Theory Study of the Role of the Copper Metalation of Azomethine Ylides in [3 + 2] Cycloaddition Reactions. *J. Org. Chem.* **2018**, *83*, 10959–10973. [[CrossRef](#)] [[PubMed](#)]
18. Domingo, L.R.; Kula, K.; Ríos-Gutiérrez, M.; Jasiński, R. Understanding the Participation of Fluorinated Azomethine Ylides in Carbenoid-type [3 + 2] Cycloaddition Reactions with Ynal Systems: A Molecular Electron Density Theory Study. *J. Org. Chem.* **2021**, *86*, 12644–12653. [[CrossRef](#)] [[PubMed](#)]
19. Domingo, L.R.; Aurell, M.J.; Pérez, P. A mechanistic study of the participation of azomethine ylides and carbonyl ylides in [3 + 2] cycloaddition reactions. *Tetrahedron* **2015**, *71*, 1050–1057. [[CrossRef](#)]
20. Aziz, Y.M.A.; Lotfy, G.; Said, M.M.; El Ashry, E.S.H.; El Tamany, E.S.H.; Soliman, S.M.; Abu-Serie, M.M.; Tebeb, M.; Yousuf, S.; Dömling, A.; et al. Design, Synthesis, Chemical and Biochemical Insights Into Novel Hybrid Spirooxindole-Based p53-MDM2 Inhibitors with Potential Bcl2 Signaling Attenuation. *Front. Chem.* **2021**, *9*, 735236. [[CrossRef](#)]
21. Islam, M.S.; Al-Majid, A.M.; Azam, M.; Verma, V.P.; Barakat, A.; Haukka, M.; Domingo, L.R.; Elgazar, A.A.; Mira, A.; Badria, F.A. Synthesis of Spirooxindole Analogs Tethered Pyrazole Scaffold as Acetylcholinesterase Inhibitors. *ChemistrySelect* **2021**, *6*, 14039–14053. [[CrossRef](#)]
22. Barakat, A.; Haukka, M.; Soliman, S.M.; Ali, M.; Al-Majid, A.M.; El-Faham, A.; Domingo, L.R. Straightforward Regio- and Diastereoselective Synthesis, Molecular Structure, Intermolecular Interactions and Mechanistic Study of Spirooxindole-Engrafted Rhodanine Analogs. *Molecules* **2021**, *26*, 7276. [[CrossRef](#)]
23. Al-Majid, A.M.; Soliman, S.M.; Haukka, M.; Ali, M.; Islam, M.S.; Shaik, M.R.; Barakat, A. Design, Construction, and Characterization of a New Regioisomer and Diastereomer Material Based on the Spirooxindole Scaffold Incorporating a Sulphone Function. *Symmetry* **2020**, *12*, 1337. [[CrossRef](#)]
24. Ríos-Gutiérrez, M.; Barakat, A.; Domingo, L.R. A Molecular Electron Density Theory Study of the pmr-type [3 + 2] Cycloaddition Reaction of Azomethine Ylides Derived from Isatins and L-Proline with Phenyl Vinyl Sulphone. *Organic* **2022**, *3*, 122–136.
25. Domingo, L.R.; Sáez, J.A.; Zaragoza, R.J.; Arnó, M. Understanding the Participation of Quadricyclane as Nucleophile in Polar Cycloadditions toward Electrophilic Molecules. *J. Org. Chem.* **2008**, *73*, 8791–8799. [[CrossRef](#)] [[PubMed](#)]
26. Domingo, L.R. A new C–C bond formation model based on the quantum chemical topology of electron density. *RSC Adv.* **2014**, *4*, 32415–32428. [[CrossRef](#)]
27. Domingo, L.R.; Perez, P.; Sáez, J.A. Understanding the local reactivity in polar organic reactions through electrophilic and nucleophilic Parr functions. *RSC Adv.* **2013**, *3*, 1486–1494. [[CrossRef](#)]
28. Astruc, D. Why is Ferrocene so Exceptional? *Eur. J. Inorg. Chem.* **2017**, *1*, 6–29. [[CrossRef](#)]

29. Harding, M.M.; Mokdsi, G. Antitumour metallocenes: Structure-activity studies and interactions with biomolecules. *Curr. Med. Chem.* **2000**, *7*, 1289–1303. [[CrossRef](#)] [[PubMed](#)]
30. Dubar, F.; Khalife, J.; Brocard, J.; Dive, D.; Biot, C. Ferroquine, an ingenious antimalarial drug—thoughts on the mechanism of action. *Molecules* **2008**, *13*, 2900–2907. [[CrossRef](#)] [[PubMed](#)]
31. Top, S.; Vessières, A.; Leclercq, G.; Quivy, J.; Tang, J.; Vaissermann, J.; Huché, M.; Jaouen, G. Synthesis, biochemical properties and molecular modelling studies of organometallic specific estrogen receptor modulators (SERMs), the ferrocifens and hydroxyferrocifens: Evidence for an antiproliferative effect of hydroxyferrocifens on both hormone-dependent and hormone-independent breast cancer cell lines. *Chem. A Eur. J.* **2003**, *9*, 5223–5236.
32. Ganesh, V.; Sudhir, V.S.; Kundu, T.; Chandrasekaran, S. 10 years of click chemistry: Synthesis and applications of ferrocene-derived triazoles. *Chem. Asian J.* **2011**, *6*, 2670–2694. [[CrossRef](#)]
33. Hillard, E.; Vessières, A.; Thouin, L.; Jaouen, G.; Amatore, C. Ferrocene-mediated proton-coupled electron transfer in a series of ferrocifen-type breast-cancer drug candidates. *Angew. Chem.* **2006**, *118*, 291–296. [[CrossRef](#)]
34. Altowyan, M.S.; Ali, M.; Soliman, S.M.; Al-Majid, A.M.; Islam, M.S.; Yousuf, S.; Choudhary, M.I.; Ghabbour, H.A.; Barakat, A. Synthesis, computational studies and biological activity of oxamohydrazide derivatives bearing isatin and ferrocene scaffolds. *J. Mol. Struct.* **2020**, *1202*, 127372. [[CrossRef](#)]
35. Ferreira, V.F.; da Rocha, D.R.; da Silva, F.C.; Ferreira, P.G.; Boechat, N.A.; Magalhães, J.L. Novel 1H-1,2,3-, 2H-1,2,3-, 1H-1,2,4- and 4H-1,2,4-triazole derivatives: A patent review (2008–2011). *Expert Opin. Ther. Pat.* **2013**, *23*, 319–331. [[CrossRef](#)] [[PubMed](#)]
36. Salmon, A.J.; Williams, M.L.; Wu, Q.K.; Morizzi, J.; Gregg, D.; Charman, S.A.; Vullo, D.; Supuran, C.T.; Poulsen, S.A. Metallocene-based inhibitors of cancer-associated carbonic anhydrase enzymes IX and XII. *J. Med. Chem.* **2012**, *55*, 5506–5517. [[CrossRef](#)] [[PubMed](#)]
37. Kumar, K.; Carrere-Kremer, S.; Kremer, L.; Guérardel, Y.; Biot, C.; Kumar, V. 1H-1,2,3-triazole-tethered isatineferrocene and isatineferrocenylchalcone conjugates: Synthesis and in vitro antitubercular evaluation. *Organometallics* **2013**, *32*, 5713–5719. [[CrossRef](#)]
38. Kumar, K.; Carrère-Kremer, S.; Kremer, L.; Guérardel, Y.; Biot, C.; Kumar, V. Azide–alkyne cycloaddition en route towards 1H-1,2,3-triazole-tethered β -lactam–ferrocene and β -lactam–ferrocenylchalcone conjugates: Synthesis and in vitro anti-tubercular evaluation. *Dalton Trans.* **2013**, *42*, 1492–1500. [[CrossRef](#)]
39. Kumar, K.; Pradines, B.; Madamet, M.; Amalvict, R.; Benoit, N.; Kumar, V. 1H-1,2,3-triazole tethered isatin-ferrocene conjugates: Synthesis and in vitro antimalarial evaluation. *Eur. J. Med. Chem.* **2014**, *87*, 801–804. [[CrossRef](#)]
40. Van Staveren, D.R.; Metzler-Nolte, N. Bioorganometallic chemistry of ferrocene. *Chem. Rev.* **2004**, *104*, 5931–5986. [[CrossRef](#)]
41. Xu, J.; Yang, Y.; Baigude, H.; Zhao, H. New ferrocene–triazole derivatives for multisignaling detection of Cu^{2+} in aqueous medium and their antibacterial activity. *Spectrochim. Acta Part A Mol. Biomol. Spectrosc.* **2020**, *229*, 117880. [[CrossRef](#)]
42. Arivazhagan, C.; Borthakur, R.; Ghosh, S. Ferrocene and triazole-appended rhodamine based multisignaling sensors for Hg^{2+} and their application in live cell imaging. *Organometallics* **2015**, *34*, 1147–1155. [[CrossRef](#)]
43. Fouda, M.F.; Abd-Elzاهر, M.M.; Abdelsamaia, R.A.; Labib, A.A. On the medicinal chemistry of ferrocene. *Appl. Organomet. Chem.* **2007**, *21*, 613–625. [[CrossRef](#)]
44. Larik, F.A.; Saeed, A.; Fattah, T.A.; Muqadar, U.; Channar, P.A. Recent advances in the synthesis, biological activities and various applications of ferrocene derivatives. *Appl. Organomet. Chem.* **2017**, *31*, e3664. [[CrossRef](#)]
45. Altowyan, M.S.; Soliman, S.M.; Haukka, M.; Al-Shaalan, N.H.; Alkharboush, A.A.; Barakat, A. Synthesis and Structure Elucidation of Novel Spirooxindole Linked to Ferrocene and Triazole Systems via [3 + 2] Cycloaddition Reaction. *Molecules* **2022**, *27*, 4095. [[CrossRef](#)] [[PubMed](#)]
46. Becke, A.D.; Edgecombe, K.E. A simple measure of electron localization in atomic and molecular systems. *J. Chem. Phys.* **1990**, *92*, 5397–5403. [[CrossRef](#)]
47. Silvi, B.; Savin, A. Classification of chemical bonds based on topological analysis of electron localization functions. *Nature* **1994**, *371*, 683–686. [[CrossRef](#)]
48. Reed, A.E.; Weinstock, R.B.; Weinhold, F. Natural population analysis. *J. Chem. Phys.* **1985**, *83*, 735–746. [[CrossRef](#)]
49. Reed, A.E.; Curtiss, L.A.; Weinhold, F. Intermolecular interactions from a natural bond orbital, donor-acceptor viewpoint. *Chem. Rev.* **1988**, *88*, 899–926. [[CrossRef](#)]
50. Parr, R.G.; Yang, W. *Density Functional Theory of Atoms and Molecules*; Oxford University Press: New York, NY, USA, 1989.
51. Domingo, L.R.; Ríos-Gutiérrez, M.; Pérez, P. Applications of the conceptual density functional indices to organic chemistry reactivity. *Molecules* **2016**, *21*, 748. [[CrossRef](#)]
52. Domingo, L.R.; Ríos-Gutiérrez, M. *Application of Reactivity Indices in the Study of Polar Diels–Alder Reactions in Conceptual Density Functional Theory: Towards a New Chemical Reactivity Theory*; Liu, S., Ed.; WILEY-VCH GmbH: Weinheim, German, 2022; Volume 2, pp. 481–502.
53. Parr, R.G.; Pearson, R.G. Absolute hardness: Companion parameter to absolute electronegativity. *J. Am. Chem. Soc.* **1983**, *105*, 7512–7516. [[CrossRef](#)]
54. Domingo, L.R.; Ríos-Gutiérrez, M.; Pérez, P. A Molecular Electron Density Theory Study of the Reactivity of Tetrazines in Aza-Diels–Alder Reactions. *RSC Adv.* **2020**, *10*, 15394–15405. [[CrossRef](#)]
55. Parr, R.G.; Szentpaly, L.V.; Liu, S. Electrophilicity index. *J. Am. Chem. Soc.* **1999**, *121*, 1922–1924. [[CrossRef](#)]

56. Domingo, L.R.; Chamorro, E.; Pérez, P. Understanding the reactivity of captodative ethylenes in polar cycloaddition reactions. A theoretical study. *J. Org. Chem.* **2008**, *73*, 4615–4624. [[CrossRef](#)]
57. Chamorro, E.; Duque-Noreña, M.; Gutiérrez-Sánchez, N.; Rincón, E.; Domingo, L.R. A Close Look to the Oxaphosphetane Formation along the Wittig Reaction: A [2 + 2] Cycloaddition? *J. Org. Chem.* **2020**, *85*, 6675–6686. [[CrossRef](#)] [[PubMed](#)]
58. Aurell, M.J.; Domingo, L.R.; Perez, P.; Contreras, R. A theoretical study on the regioselectivity of 1,3-dipolar cycloadditions using DFT-based reactivity indexes. *Tetrahedron* **2004**, *60*, 11503–11509. [[CrossRef](#)]
59. Benchouk, W.; Mekelleche, S.M.; Silvi, B.; Aurell, M.J.; Domingo, L.R. Understanding the kinetic solvent effects on the 1,3-dipolar cycloaddition of benzonitrile N-oxide: A DFT study. *J. Phys. Org. Chem.* **2011**, *24*, 611–618. [[CrossRef](#)]
60. Domingo, L.R.; Ríos-Gutiérrez, M.; Pérez, P. How does the global electron density transfer diminish activation energies in polar cycloaddition reactions? A Molecular Electron Density Theory study. *Tetrahedron* **2017**, *73*, 1718–1724. [[CrossRef](#)]
61. Lefebvre, C.; Rubez, G.; Khartabil, H.; Boisson, J.C.; Contreras-García, J.; Hénon, E. Accurately extracting the signature of intermolecular interactions present in the NCI plot of the reduced density gradient versus electron density. *Phys. Chem. Chem. Phys.* **2017**, *19*, 17928–17936. [[CrossRef](#)] [[PubMed](#)]
62. Lefebvre, C.; Khartabil, H.; Boisson, J.-C.; García, J.C.; Piquemal, J.-P.; Hénon, E. The independent gradient model: A new approach for probing strong and weak interactions in molecules from wave function calculations. *Chem. Phys. Chem.* **2018**, *19*, 724–735. [[CrossRef](#)]
63. Klein, J.; Khartabil, H.; Boisson, J.-C.; Contreras-García, J.; Piquemal, J.P.; Hénon, E. New Way for Probing Bond Strength. *J. Phys. Chem. A* **2020**, *124*, 1850–1860. [[CrossRef](#)]
64. Ponce-Vargas, M.; Lefebvre, C.; Boisson, J.-C.; Hénon, E. Atomic Decomposition Scheme of Noncovalent Interactions Applied to Host-Guest Assemblies. *J. Chem. Inf. Model.* **2020**, *60*, 268–278. [[CrossRef](#)]
65. Chai, J.-D.; Head-Gordon, M. Long-range corrected hybrid density functionals with damped atom–atom dispersion corrections. *Phys. Chem. Chem. Phys.* **2008**, *10*, 6615–6620. [[CrossRef](#)]
66. Hehre, M.J.; Radom, L.; Schleyer, P.V.R.; Pople, J. *Ab Initio Molecular Orbital Theory*; Wiley: New York, NY, USA, 1986.
67. Schlegel, H.B. Optimization of equilibrium geometries and transition structures. *J. Comput. Chem.* **1982**, *3*, 214–218. [[CrossRef](#)]
68. Schlegel, H.B. *Modern Electronic Structure Theory*. Yarkony, D.R., Ed.; World Scientific Publishing: Singapore, 1994.
69. Fukui, K. Formulation of the reaction coordinate. *J. Phys. Chem.* **1970**, *74*, 4161–4163. [[CrossRef](#)]
70. González, C.; Schlegel, H.B. Reaction path following in mass-weighted internal coordinates. *J. Phys. Chem.* **1990**, *94*, 5523–5527. [[CrossRef](#)]
71. González, C.; Schlegel, H.B. Improved algorithms for reaction path following: Higher-order implicit algorithms. *J. Chem. Phys.* **1991**, *95*, 5853–5860. [[CrossRef](#)]
72. Tomasi, J.; Persico, M. Molecular interactions in solution: An overview of methods based on continuous distributions of the solvent. *Chem. Rev.* **1994**, *94*, 2027–2094. [[CrossRef](#)]
73. Simkin, B.Y.; Sheikhet, I.I. *Quantum Chemical and Statistical Theory of Solutions—Computational Approach*; Ellis Horwood: London, UK, 1995.
74. Cossi, M.; Barone, V.; Cammi, R.; Tomasi, J. Ab initio study of solvated molecules: A new implementation of the polarizable continuum model. *Chem. Phys. Lett.* **1996**, *255*, 327–335. [[CrossRef](#)]
75. Cancès, E.; Mennucci, B.; Tomasi, J. A new integral equation formalism for the polarizable continuum model: Theoretical background and applications to isotropic and anisotropic dielectrics. *J. Chem. Phys.* **1997**, *107*, 3032–3041. [[CrossRef](#)]
76. Barone, V.; Cossi, M.; Tomasi, J. Geometry optimization of molecular structures in solution by the polarizable continuum model. *J. Comput. Chem.* **1998**, *19*, 404–417. [[CrossRef](#)]
77. Frisch, M.J.; Trucks, G.W.; Schlegel, H.B.; Scuseria, G.E.; Robb, M.A.; Cheeseman, J.R.; Scalmani, G.; Barone, V.; Petersson, G.A.; Nakatsuji, H.; et al. *Gaussian 16, Revision A.03*; Gaussian, Inc.: Wallingford, CT, USA, 2016.
78. Noury, S.; Krokidis, X.; Fuster, F.; Silvi, B. Computational tools for the electron localization function topological analysis. *Comput. Chem.* **1999**, *23*, 597–604. [[CrossRef](#)]
79. Dennington, R.; Keith, T.A.; Millam, J.M. *GaussView*, 6th ed.; Semichem Inc.: Shawnee, KS, USA, 2016.